SAND2015-1024C

Stress-life Model Sensitivity to Cycle Counting Methods for a Printed Circuit Board Subjected to Random Excitation

Troy Savoie, Vit Babuška
Sandia National Laboratories*
Albuquerque, NM 87185

ABSTRACT

Fatigue failure models, such as Miner's Method, rely on stress-life models notably *S-N* curves. Usually stress-life models are generated from a series of experiments in which a specimen is subjected to single frequency cyclic loading. This paper describes a two-step method for generating stress-life models from random vibration data. The sensitivity of the stress life model to failure type, measurement location, cycle counting methods, and response distribution parameters was explored. The method was developed and demonstrated for functional failure of a printed circuit board subjected to random vibration excitation. Experiments showed that the definition of damage inducing cycles depends on the failure mode; that measurement location affects the stress life model because of the spatial stress variations in the specimen under test; peak-to-peak cycles produced more conservative S-N curves than rainflow cycles; and including higher order response characteristics may produce more accurate stress-life models.

I. INTRODUCTION

Miner's method [1] is a relatively simple, non-parametric method for estimating fatigue life. It is based on the assumption that every structural component has a specific fatigue life and every stress cycle uses up a portion of that fatigue life. Furthermore, it assumes fatigue damage is proportional to the work absorbed by the structure [1]. Miner's method is specified in almost every design code because of its simplicity and because the engineering community has not found anything consistently better ([2], pg. 271).

To use Miner's method, an *S-N* curve, also called a stress-life model, is required. A typical *S-N* curve is shown in Figure 1. *S-N* curves can be found in handbooks for specific materials and test conditions. For example, MIL-HDBK-5 [3] contains properties, including *S-N* curves, for many steels and alloys. Usually stress-life models are generated from a series of experiments in which a specimen is subjected to single frequency cyclic loading until complete separation of the specimen ([3], pg. 9-219).

In this paper, an *S-N* stress life model of a printed circuit board (PCB) is derived from random vibration tests. The PCB has four signal generator circuits (Figure 2). Two circuits generate sinusoidal signals and two generate square wave signals. Failure is defined as failure of a circuit, which is likely caused by a structural failure of a component on the PCB, or of traces in the PCB itself.

*Sandia National Laboratories is a multi-program laboratory managed and operated by Sandia Corporation, a wholly owned subsidiary of Lockheed Martin Corporation, for the U.S. Department of Energy's National Nuclear Security Administration under contract DE-AC04-94AL85000.

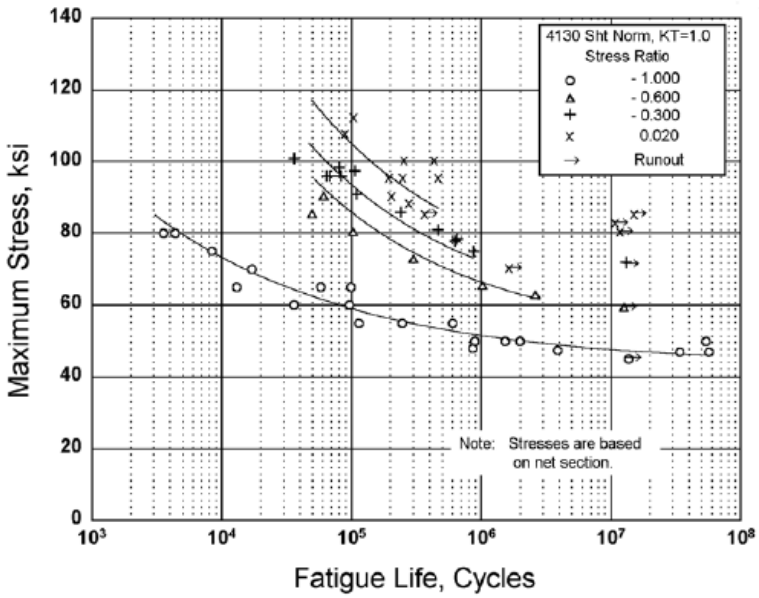

Figure 2.3.1.2.8(a). Best-fit S/N curves for unnotched 4130 alloy steel sheet, normalized, longitudinal direction.

Figure 1 Example *S-N* curve for alloy steel from MIL-HDBK-5

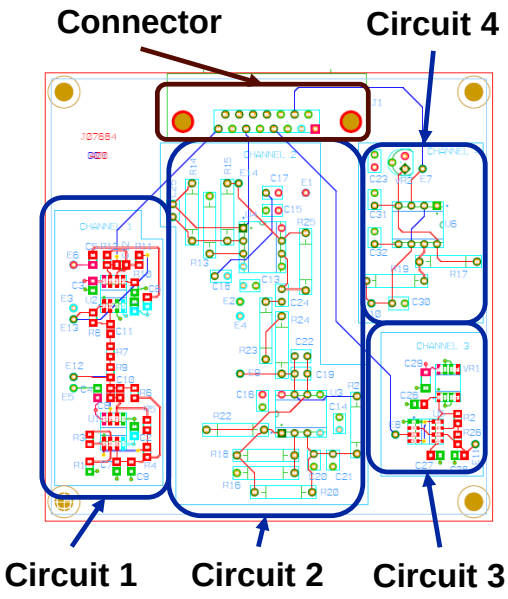

Figure 2 PCB and the locations of the 4 circuits

Because of the functional failure aspect of this project, no stress-life model was available for the PCB. A previous paper [4] described a RMS stress life model of the PCB derived from the random vibration data. Since stress life models typically relate stress amplitude or maximum tensile stress, rather than RMS stress, to fatigue life, a method for generating a damage equivalent sinusoidal stress amplitude *S-N* model was developed and is described in this paper. In the RMS stress life model, only the number of cycles to failure is needed. To derive an *S-N*

curve from random data the stress amplitude distribution is required, not just the number of cycles to failure. The stress amplitude distribution is a function of the response bandwidth and the way stress cycles are defined. The sensitivity of the *S-N* curve to these parameters is discussed.

Section II provides a brief overview of Miner's method and key features of stress-life models applicable to this project are summarized in Section III. A two-step method for deriving *S-N* curves from random vibration data is described in Section IV. Section V contains a description of the experimental configuration and data collection. The experimental results from a random vibration test of 16 PCBs, as well as analyses of the data to identify the sensitivity of the stress life model to failure type, measurement location, cycle counting methods, and response distribution are explained in Section VI. Conclusions are presented in Section VII.

II. MINER'S METHOD

Miner's method assumes fatigue damage is accumulated linearly and is proportional to energy absorbed by the structure. The basic model for fractional damage accumulation is:

$$D = \sum_{j=1}^{M} \frac{n_j}{N_j} \tag{1}$$

where

$D =$ fraction of consumed fatigue life;
$n_j =$ number of cycles experienced by the structure at stress S_j;
$N_j =$ number of cycles to failure at stress S_j determined from *S-N* curves.

In theory, failure is predicted to occur when $D = 1$; however, standard design practice uses $D < 1$. For example, $D = 0.3$ for critical life-cycle electronic systems like those on man-rated space vehicles and $D = 0.7$ for typical electronic structures ([5], pg. 410). This design practice is used because Miner's method is not consistently conservative since it does not use any parameters of the environment and failure modes explicitly. For example, since Miner's method does not account for the order of applied stress, it may over predict the fatigue life of a part that experiences the majority of large stress cycles early. A part will be more likely to fail earlier in this type of environment than one that experiences a random distribution of stress cycles.

Miner's Method is widely used with some common assumptions:

a. Eq. (1) is failure definition specific;
b. The amount of damage from a cycle only depends on the number of cycles to failure at the applied load amplitude for that cycle;
c. The amount of damage from a load cycle is independent of the total life consumed prior to application of the load cycle or the magnitude of previous loading.

Use of Miner's method requires an *S-N* curve and knowing the number of cycles the structure experiences in its operating environment.

III. STRESS LIFE MODELS

Stress-life models are always derived from sinusoidal, full reversal cyclic loading tests of specimens to complete separation. Four inherent aspects related to the stress side of *S-N* curves are:

a. the *S-N* curve is consistent with the operational stress field in the structure;
b. the *S-N* curve is failure mode and failure definition specific;
c. the *S-N* curve assumes zero mean stress – a non-zero mean tensile stress will reduce fatigue life while a non-zero mean compressive stress will increase apparent fatigue life;
d. the *S-N* curve is material specific - the specific material at risk of fatigue failure is known.

On the fatigue life side, the number of cycles is straightforward to determine for cyclic and narrowband response. It is not so straightforward to define and count stress cycles for wide band response.

A simplifying assumption in fatigue analysis is that fatigue strength obeys a power law relationship:

$$NS^b = S_1^b \tag{2}$$

where N is the number of cycles to failure, S is the cyclical stress amplitude, b is the fatigue strength coefficient (i.e., $-1/b$ is the slope of the *S-N* line in log-log space), and S_1 is the single cycle ultimate (or flexural) strength. Both b and S_1 are empirically derived constants, whereas N and S are measured during test.

The power law model in Eq. (2) originated from fatigue tests on metals. It is sometimes referred to as Basquin's equation and is based on observations that fatigue failure is fundamentally due to microscopic cracks initiated at stress concentration features that eventually reach a critical size and affect the structural properties of the material (from loss of stiffness to fracture). Note that Eq. (2) requires $S > 0$ for arbitrary b.

The fatigue strength relationship in the form of Eq. (2) is used in this paper because the structural failure leading to circuit failure is a crack in a circuit trace in the PCB or a crack in an electrical component, both of which are metal material failures. Equation (2) is a linear function in log-log space and is often written as:

$$\hat{S} = \widehat{S_1} - \frac{1}{b}\widehat{N} \tag{3}$$

where $\widehat{N} = \log_{10} N$, $\hat{S} = \log_{10} S$, and $\widehat{S_1} = \log_{10} S_1$. The number of cycles, N, and the stress amplitude, S, are measured and $\widehat{S_1}$ and b can be readily obtained by least squares estimation.

Because there is a distribution of stresses in a structure experiencing random vibration, consider the continuous form of Eq. (1):

$$D = \int_0^\infty \frac{n(S)}{N(S)} dS \tag{4}$$

Let $n(S) = N_T f(S)$ where $f(S)$ is the probability density function (PDF) of the stress peak amplitude and $N(S)$ is the number cycles to failure at stress S, and N_T is the total number of cycles to failure. Substituting the power law relationship, Eq. (2), for $N(S)$ into Eq. (4) gives:

$$D = \frac{N_T}{S_1^b} \int_0^\infty S^b f(S) dS \tag{5}$$

The integral term in Eq. (5) is the order b moment of the peak stress distribution:

$$E[S^b] = \int_0^\infty S^b f(S) dS \tag{6}$$

For $D = 1$, Eq. (5) becomes

$$N_T E[S^b] = S_1^b \tag{7}$$

If the response is narrowband the instantaneous stress has a Gaussian PDF, and the probability density function (PDF) of the stress amplitude is a Rayleigh distribution:

$$f(S) = \frac{S}{\sigma^2} e^{\left(\frac{-S^2}{2\sigma^2}\right)} \tag{8}$$

where σ is the stress standard deviation (RMS when the stress distribution is zero mean), and:

$$E[S^b] = \left(\sqrt{2}\sigma\right)^b \Gamma\left(\frac{b}{2} + 1\right), \; b > 0 \tag{9}$$

Substitution of $E[S^b]$ from Eq. (9) into Eq. (7) gives a power law RMS stress life model i.e., a $\sigma - N_T$ curve, in terms of stress standard deviation and number of cycles to failure for narrow band random vibration:

$$N_T \sigma^b = \frac{S_1^b}{\left(\sqrt{2}\right)^b \Gamma\left(\frac{b}{2} + 1\right)} \tag{10}$$

Recalling that the relationship between the peak amplitude and the standard deviation of a sine wave is $S = \sqrt{2}\sigma$ gives:

$$N_T \hat{S}_e^b = S_1^b \tag{11}$$

where

$$\hat{S}_e = S_e \left(\Gamma\left(\frac{b}{2}+1\right)\right)^{1/b} = S_e \lambda \tag{12}$$

is the equivalent stress amplitude and $S_e = \sqrt{2}\sigma$ is the effective sinusoidal amplitude. Equation (12) links stress from narrowband random vibration to sinusoidal *S-N* curves. The term $\lambda = \left(\Gamma\left(\frac{b}{2}+1\right)\right)^{1/b}$ is a factor that accounts for the distribution of stress amplitude in the narrow band random response. It scales the effective sinusoidal amplitude by a factor ranging from 0.89 to 1.73 depending on the value of b, to give an equivalent stress amplitude that has the same damage potential as the random stress field. The implication is that fatigue life in narrow band random vibration can be computed very simply with Miner's rule with existing, handbook *S-N* curves. For example, for metals, $b \cong 6$, which suggests using 2σ stresses with published *S-N* curves. Using 3σ stresses will be sufficiently conservative even if b is quite uncertain. Note that this approach is rather more conservative than Steinberg's 3-term Miner's method [5].

For wide band response, the stress amplitude distribution is not Rayleigh. A measure of the bandwidth of a random process is the irregularity factor. When the stress distribution, $s(t)$, is Gaussian, the irregularity factor, α, is:

$$\alpha = \frac{\left(\int_0^\infty f^2 W_{SS}(f) df\right)^2}{\left(\int_0^\infty W_{SS}(f) df\right)\left(\int_0^\infty f^4 W_{SS}(f) df\right)} \tag{13}$$

where $W_{SS}(f)$ is the spectral density of the response, i.e., stress measurement. The distribution of amplitude peaks in a general random process is the Rice distribution [2]:

$$f(S) = \frac{\sqrt{1-\alpha^2}}{\sigma\sqrt{2\pi}} e^{\left(\frac{-S^2}{2\sigma^2(1-\alpha^2)}\right)} + \alpha\Phi\left(\frac{\alpha}{\sigma\sqrt{1-\alpha^2}}S\right)\frac{S}{\sigma^2} e^{-\frac{1}{2}\left(\frac{S}{\sigma}\right)^2} \tag{14}$$
$$-\infty < S < \infty$$

where Φ is the Gaussian cumulative distribution. This is a generalization of the Rayleigh distribution as a function of the irregularity factor. The first term has the form of a Gaussian distribution, the second has the form of a Rayleigh distribution multiplied by the Gaussian cumulative distribution. Note that unlike a Rayleigh distribution, the second term is not zero for $S < 0$. A random process is perfectly narrow-band when $\alpha = 1$ and it is infinitely wide (i.e., white) when $\alpha = 0$. The standard Rice distribution is shown in Figure 3 with $\sigma = 1$. Note that the Rayleigh distribution has a longer, larger tail than a normal distribution. That is why the narrow band assumption leads to a conservative estimate of fatigue damage.

The Rice distribution is not as useful as it might appear. The assumption that the number of stress reversals is one-to-one with the number of stress peaks does not hold for a wide band process. Miner's method and the power law stress life model require only positive (i.e., tensile) stress peaks, $S > 0$, (Eq. (2)) because of the implicit assumption that compression only cycles cause no damage. Note that compression cycles contribute to fatigue damage accumulation only

when there is localized tensile stress and this failure location may not be the same as the one most sensitive to global tensile stress. However, the Rice distribution is helpful toward understanding stress distribution from random vibration.

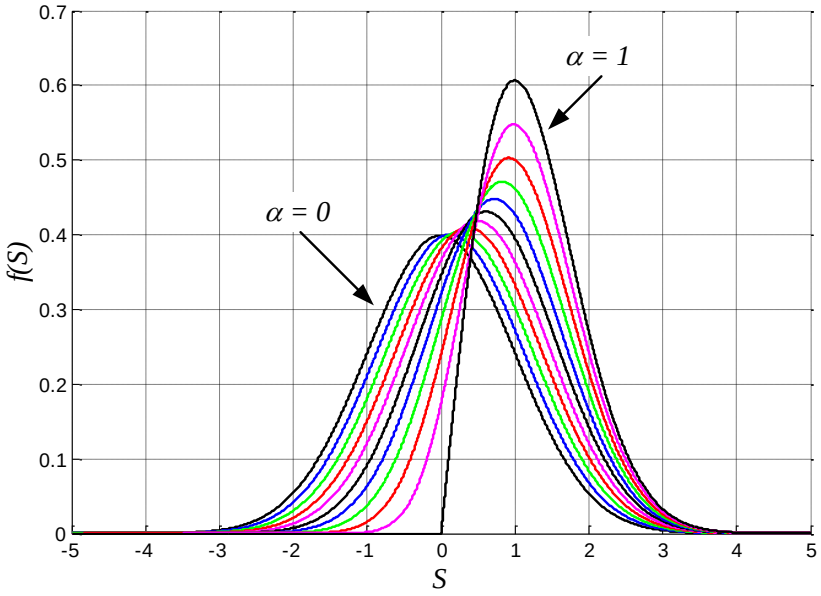

Figure 3 The Rice distribution, $-\infty < S < \infty$

For the PCB, assume that the top of the board is instrumented with strain gages. Assume that the neutral axis is at the mid-plane of the board and out-of-plane bending is the dominant deflection type, so while the top of the board is in compression the bottom is in tension, and vice versa. Assume further that failure could be in the cross-section above or below the neutral axis. If the board failure mode is due to normal stress, then only half of the cycles are damage causing cycles. In this case, the Rice distribution is truncated to only $S > 0$ (Figure 4), which is consistent with Eq. (6). The truncated Rice distribution also applies to component failure on one side of the board, under the assumption that the component does not see fatigue damage inducing stresses when its side of the board is in compression.

If the failure mode is inter-laminar shear, then both compression and tension cause damage equally. Therefore, Eq. (6) becomes:

$$E[S^b] = \int_{-\infty}^{\infty} |S|^b f(S) dS \tag{15}$$

This is equivalent to folding the Rice distribution as shown in Figure 5.

The RMS stress amplification factors ($\sqrt{2}\lambda$, Eq. (12)) for the truncated Rice distribution and the folded Rice distribution are shown in Figure 6 and Figure 7, respectively for irregularity factors, $0 \leq \alpha \leq 1$.

In a previous paper [4], a $\sigma - N_T$ stress life model was derived for the PCB from random vibration tests of 16 boards. In the next section, an *S-N* stress life model in the form of Eq. (11) is derived from random vibration test data using Eqs. (6) and (7). The sensitivity of the resulting *S-N* curve to the cycle counting method is illustrated numerically.

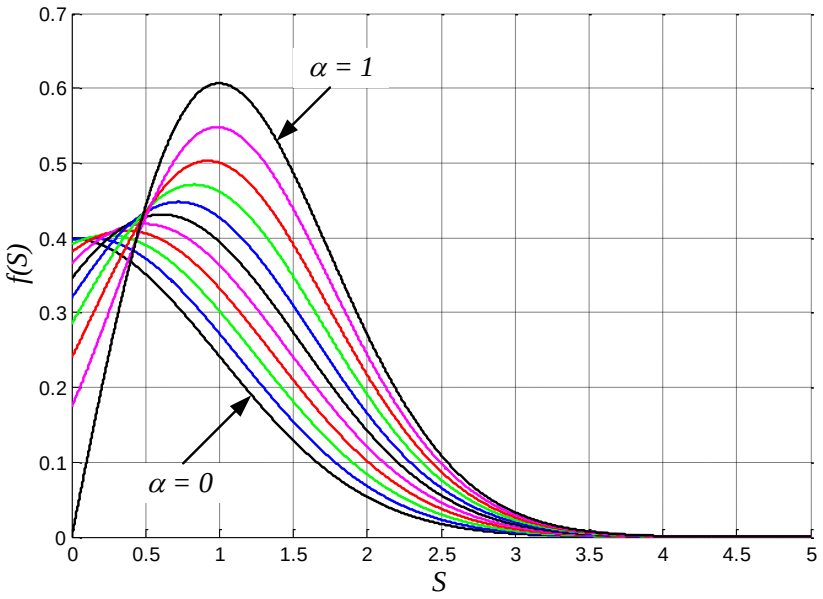

Figure 4 The Rice distribution, *S > 0*

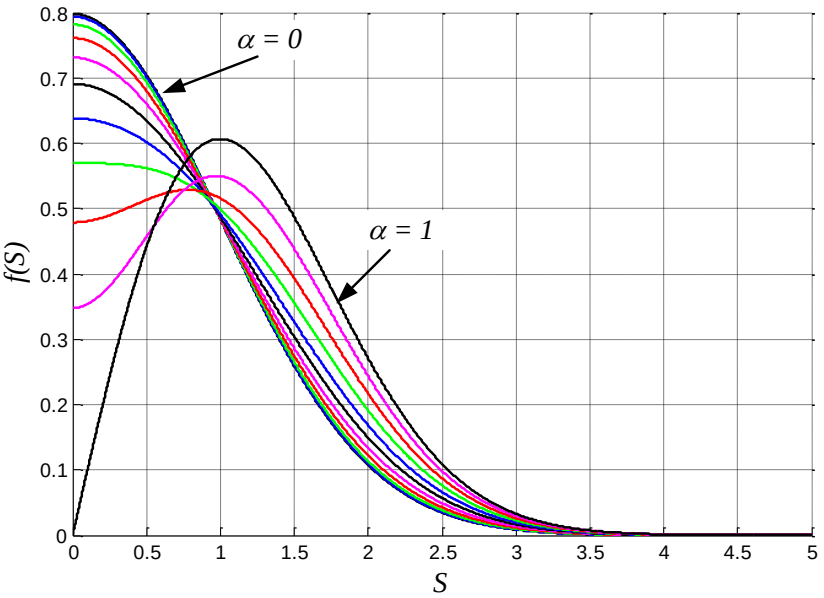

Figure 5 The folded Rice distribution *S > 0*

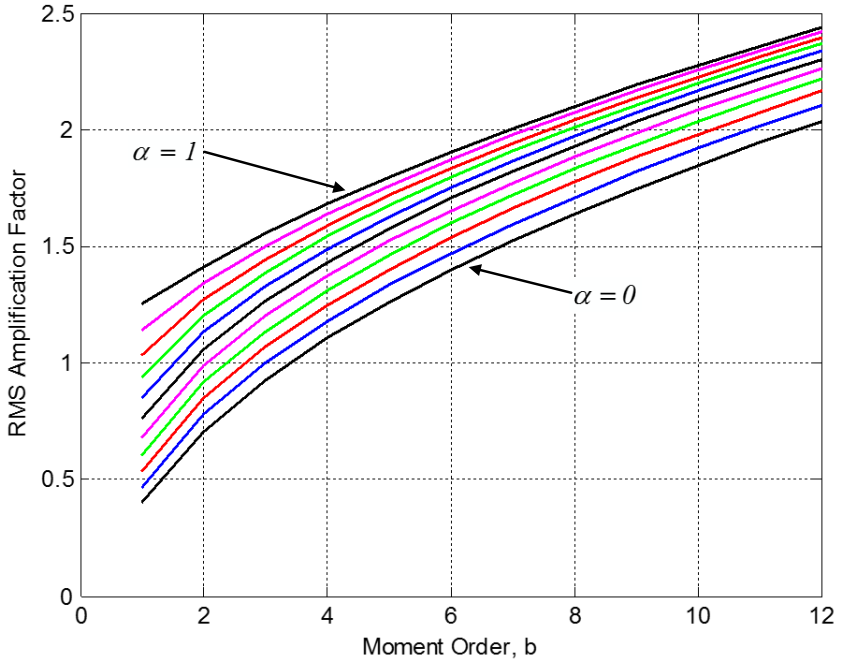

Figure 6 Truncated Rice distribution RMS amplification factor, $\sqrt{2}\lambda$

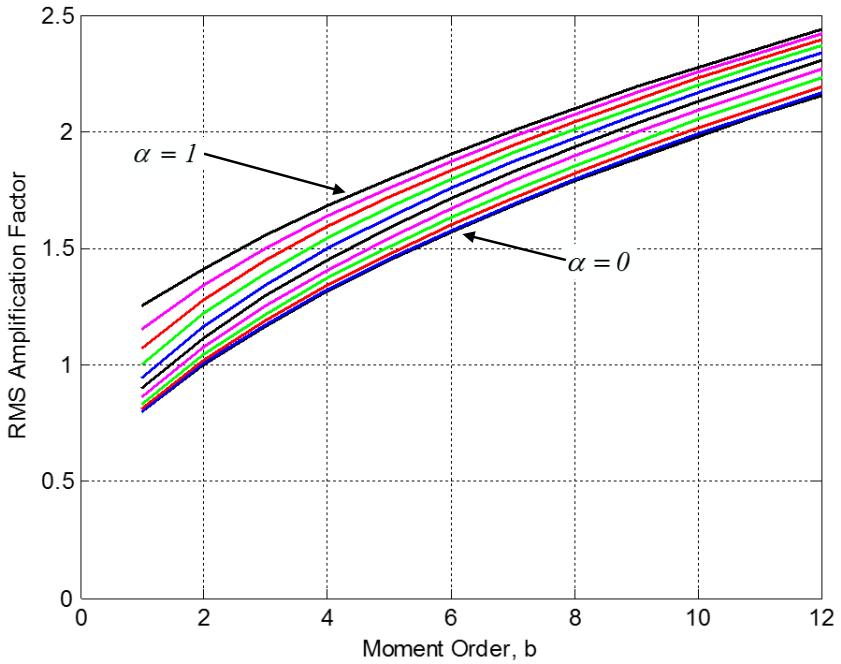

Figure 7 Folded Rice distribution RMS amplification factor, $\sqrt{2}\lambda$

IV. STRESS LIFE MODELS FROM RANDOM VIBRATION DATA

This section describes a two–step method of deriving an *S-N* curve from random vibration data. Direct identification of the parameters of the fatigue strength function in Eq. (7) does not lend itself to a straightforward least squares approach because the moment order, b, must be estimated. To that end, assume that the exponent b, in the $\sigma - N_T$ model:

$$N_T \sigma^b = C \tag{16}$$

is the same as in the *S-N* model. The model parameters, C and b, are determined empirically from measurements of σ and N_T through least squares estimation as:

$$\begin{Bmatrix} b \\ \hat{C} \end{Bmatrix} = [\Psi^T \Psi]^{-1} \Psi^T \{\hat{N}_T\} \tag{17}$$

where $\hat{C} = \log_{10} C$, $\hat{\sigma} = \log_{10} \sigma$, $\hat{N}_T = \log_{10} N_T$

$$\{\hat{N}_T\} = [\hat{N}_{T1} \quad \hat{N}_{T2} \quad \ldots \quad \hat{N}_{T1l}]^T \tag{18}$$

and

$$\Psi = \begin{bmatrix} -\hat{\sigma}_1 & 1 \\ -\hat{\sigma}_2 & 1 \\ \vdots & \vdots \\ -\hat{\sigma}_l & 1 \end{bmatrix} \tag{19}$$

Note that the RMS of a random process is not a unique descriptor of the random process. Random processes can have the same RMS yet vastly different spectral content and the spectral content may affect fatigue life as much as the overall level. Therefore, another inherent assumption herein is that the spectral content of the response from which the fatigue data are gathered is consistent with the spectral content the part experiences in its operational environment. When deriving functional fatigue failure models from random vibration data, the familiar adage "test as you fly" is sage advice.

Now, with the exponent, b, known, compute $E[S^b]$ with Eq. (6). The stress amplitude distribution, $f(S)$, must be determined by counting stress cycles in the response history. A variety of methods for counting the number of cycles in a response history have been proposed for fatigue life analyses. Each defines a cycle differently, but the objective is the same – to reduce an irregular time history of a random process into a distribution of stress ranges and amplitudes. The simplest method counts peak-to-peak cycles. A peak-to-peak cycle is the signal between two adjacent extremal points of the same type – a peak or a valley. The rainflow method [6], [7] which counts closed stress/strain hysteresis loops is the industry standard for counting the number of stress cycles, determining the stress range and the mean stress for each cycle in a realization of a random process. For narrowband random response dominated by a single mode, rainflow cycles and peak-to-peak cycles are the same. Regardless of the method and cycle definition used, the total number of cycles in the response history will be the same, or very nearly so; however, the rainflow stress distribution generally has a higher percentage of

large amplitude cycles than the peak-to-peak distribution. The sensitivity of the PCB stress life model to the distribution of peak amplitude stresses is compared by computing $E[S^b]$ with peak-to-peak cycles, and rainflow cycles.

Next, let $\hat{S}_e = E[S^b]^{1/b} = \lambda S_e$ from Eqs. (7), (11) and (12). This is the equivalent cyclic stress amplitude in the *S-N* curve. The last step is to estimate S_1 in Eq. (7). This is simply the mean of ${N_T}^{1/b}\hat{S}_e$ over the experiments; in this case the 16 PCB tests. The coefficient of variation of S_1 is:

$$CoV(S_1) = \frac{\sqrt{\sum_{i=1}^{M}\left[S_1 - \left({N_T}^{1/b}\hat{S}_e\right)_i\right]^2}}{S_1} \tag{20}$$

In summary, the steps to derive an *S-N* curve from random data are:

1) find the least squares estimate of b and C, using measurements of σ and N_T and Eqs. (17) - (19);
2) compute $E[S^b]$ with Eq. (6) or Eq. (15) [Note that the choice depends on the expected failure mode and the result depends on the cycle counting method];
3) Compute the equivalent cyclic stress, $\hat{S}_e$;
4) estimate S_1 in Eq. (7) – i.e., the mean of ${N_T}^{1/b}\hat{S}_e$ over the experiments

The fundamental assumptions in this method are:

1) the exponent b, in the $\sigma - N_T$ model, is the same as in the *S-N* model;
2) the spectral content of the response from which the fatigue data are gathered is consistent with the spectral content the part experiences in its operational environment.

V. THE PCB EXPERIMENTS

In the PCB fatigue study, 16 boards were available and tests had to provide data for multiple purposes so random vibration tests were used exclusively; no sinusoidal environments were applied. The boards were subjected to random vibration imparted through an electrodynamic shaker. The boards were attached to the base at two corners as shown in Figure 8. The PCB and base were mounted on an Unholtz-Dickie T-2000 shaker (Figure 9) and excited in the vertical direction over a bandwidth of 40 Hz to 2000 Hz. One accelerometer was mounted to the connector and a second was attached at a free corner.

The PCBs are square; each side is 3.5 in long. Each PCB has four signal generator circuits. Two circuits generate sinusoidal signals and two generate square wave signals (Figure 10). Failure is defined as failure of a circuit, based on the output signal from the PCB. Specifically, the per circuit failure criterion is that the peak response in three consecutive 20 second segments deviates from the peak response in the reference segment by more than 1%. The second segment in the healthy circuit is the reference segment. Figure 11 illustrates the criteria for Circuit 1. In Figure 11(a) the green dots are segments where the peak amplitude is within 1% of the reference segment peak amplitude; the blue dots are segments in which the peak amplitude exceeds the 1% threshold but they are not consecutive; the red dots are segments in which Circuit 1 has failed.

Figure 11(b) shows the output signal of Circuit 1 in the reference segment and the first failed segment. Even in the failed segment, the circuit output is qualitatively similar to the signal in the reference segment indicating that the circuit has not yet failed catastrophically.

The PCB also was instrumented with strain gages. Three strain gages were mounted along the diagonal connecting the mounting points. One was near the center of the board and the other two were near each mounting post. The accelerometer and strain gage output signals were sampled throughout the entire test at 8192 Hz. The stress amplitude distribution, $f(S)$, and number of cycles to failure, N_T, were determined from the time history of the strain response. Average stress, σ_{AVG},

$$\sigma_{AVG} = \frac{E}{2}\left[\frac{\varepsilon_1 + \varepsilon_3}{1 - \upsilon}\right] \tag{1}$$

derived from the strain gages at the corners were the quantities of interest (Figure 12). They were selected because an analysis of the circuit 1 failures indicated that they were caused by damage in the FR-4 laminate, not by damage to the electronic components. The same failure mode was assumed for circuit 4.

A quasi-isotropic Young's modulus and Poisson's ratio for the PCB were determined through static tests and were found to be: $E = 3.795x10^6\ psi$, $\upsilon = 0.266$. The board to board variation in modal properties is shown in the scatter plot of transmissibility peaks (Figure 13) measured by the accelerometer attached at a free corner of the PCB. The divisions in Figure 13 correspond to the five divisions of the 2-level fractional factorial design matrix shown in Figure 14. This design was chosen based on the board response to a flat random vibration input of $0.001\ g^2/Hz$ over 20 to 2000 Hz, which revealed four well-separated resonances with transmissibility peaks above 1 and a high-frequency band with many resonances having transmissibility peaks generally below 1. Input profiles were designed to excite the test board in these five frequency bands with prescribed combinations of high or low modal energy according to the design matrix. The high input level was $1\ g^2/Hz$ and the low input level was 6dB below this, or $0.25\ g^2/Hz$. Figure 14 shows PSD plots of three representative input profiles and the corresponding rows in the design matrix.

Each of the sixteen boards was exposed to its unique excitation profile. The tests were carried out in two phases. The initial tests were performed in 2013 and the results are described in Ref. [4]. A second series of tests was carried out in 2014. In the initial tests, none of the circuits failed in two hours in four of the DOE load profiles (DOE trials 2,5,9,10). Two boards failed prematurely in 2 initial trials (DOE trials 1, 8) so these were repeated with different boards. In one trial (DOE trial 14), it appeared that the connector block failed so this profile was rerun with a new board. All tests were performed until circuit 1 and circuit 4 failed. Only in DOE trial 4 did circuit 4 not fail. This test was terminated after 4 hours.

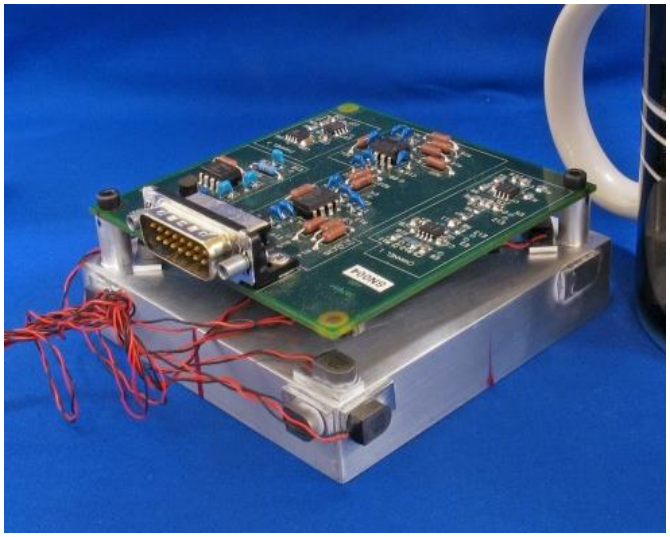

Figure 8 PCB attached to its fixture at 2 corners as tested

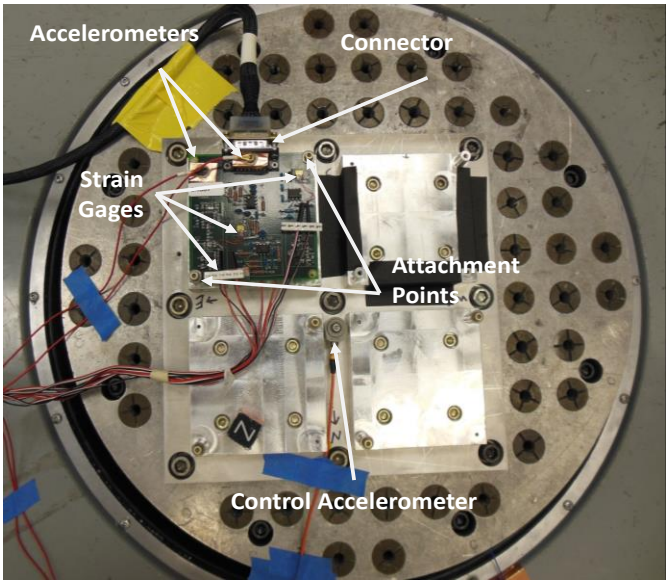

Figure 9 Vibration test instrumentation

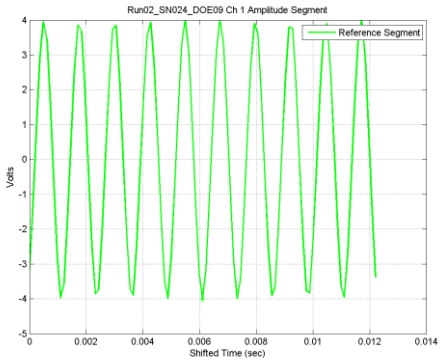

(a) Circuit 1

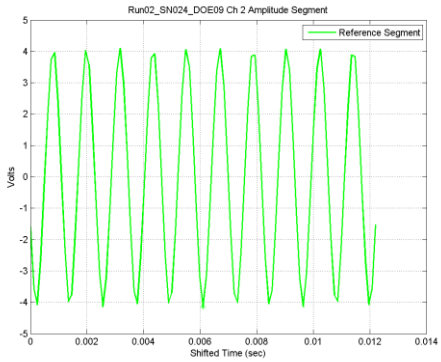

(b) Circuit 2

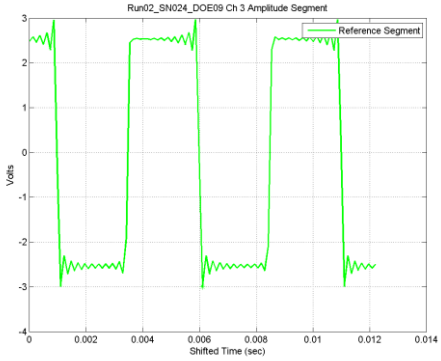

(c) Circuit 3

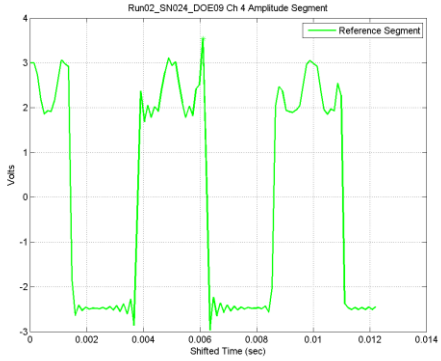

(d) Circuit 4

Figure 10 Output voltage signals from the 4 PCB circuits

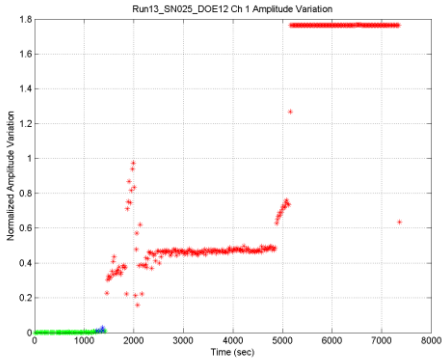

(a) Circuit 1 Normalized Amplitude Variation Time History

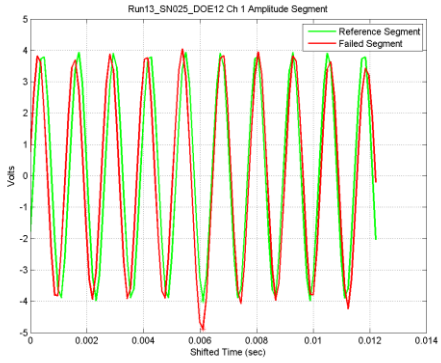

(b) Circuit 1 Output Signal in Reference Segment and First Failed Segment

Figure 11 Failure of PCB circuit 1

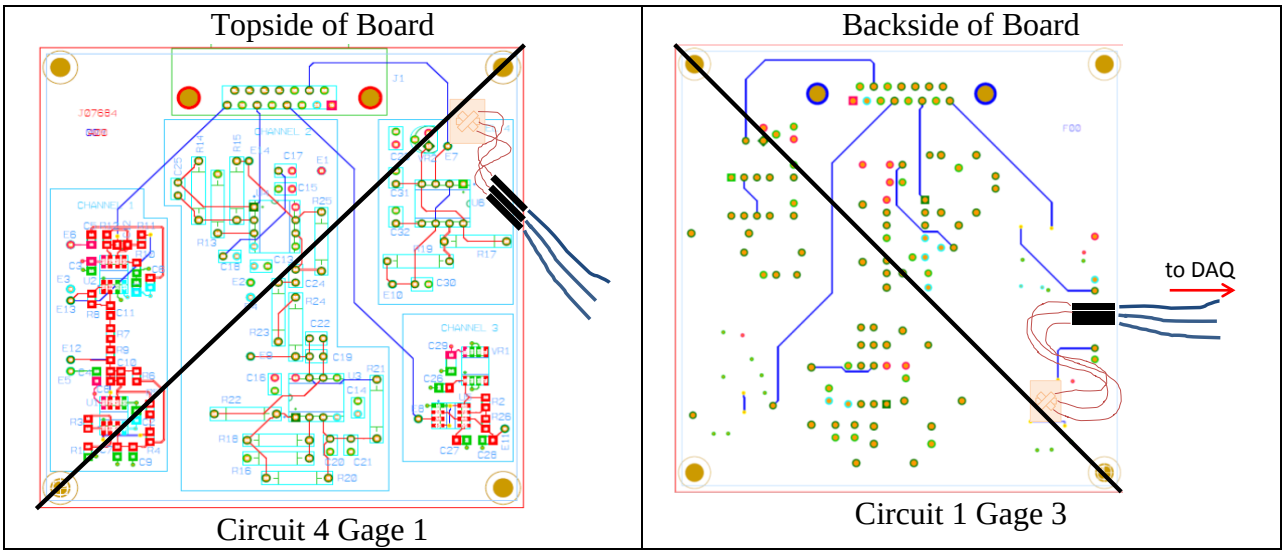

Figure 12: Strain gage locations on the PCB

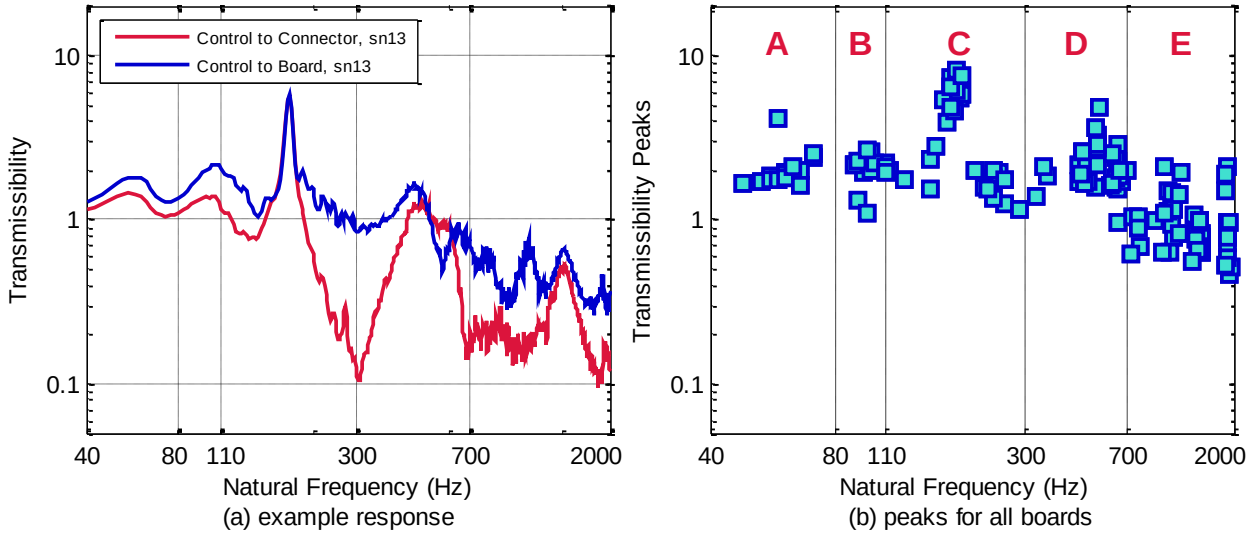

Figure 13 Transmissibility peak distribution

2_V^{5-1} Design Matrix

DOE Trial	Run	A	B	C	D	E
1	1	–	–	–	–	+
2	6	–	–	–	+	–
3	3	–	–	+	–	–
4	4	–	–	+	+	+
5	15	–	+	–	–	–
6	12	–	+	–	+	+
7	7	–	+	+	–	+
8	16	–	+	+	+	–
9	2	+	–	–	–	–
10	9	+	–	–	+	+
11	8	+	–	+	–	+
12	13	+	–	+	+	–
13	14	+	+	–	–	+
14	5	+	+	–	+	–
15	11	+	+	+	–	–
16	10	+	+	+	+	+
7*	17	–	+	+	–	–

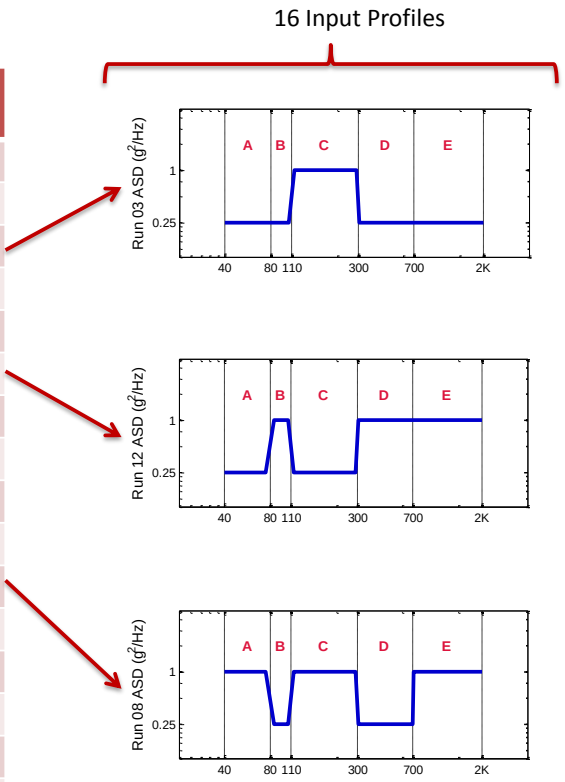

Figure 14: Two-level fractional factorial design matrix with three example profiles. The plus symbol (+) indicates high-level random vibration input in the frequency band and the minus symbol (–) indicates low-level input.

VI. RESULTS

Table 1 summarizes circuit 1 and circuit 4 times-to-failure (minutes) and the input and output RMS levels for each of the cases (G's and psi, respectively). Circuits 2 and 3 proved to be very robust and did not fail in about 50% of the tests, probably because they are not in high stress regions on the PCB. These circuits are not analyzed in this paper. Run 17 in Table 1 is a variation on Run 07 in which the input level in band E (700 Hz – 2000 Hz) was low (Figure 14). This case does not fit into the design of experiments matrix but is valid for the analyses herein.

The gage 3 $\sigma - N_T$ stress life models for circuits 1 and 4 are shown in Figure 15. The number of cycles to failure, N_T, was computed from the time histories by counting stress reversals. The stress life exponent is 4.6 and the single cycle failure stress is 10 kpsi for circuit 1. These are well below the flexural strength of FR-4 (70 kpsi). This is not surprising since the failure criterion was functional failure of the circuit, not catastrophic structural failure of the FR-4. The circuit 1 stress life model correlates well with gage 3 ($R^2 = 0.74$). The results for circuit 4 were affected by the no failure of Run 04. This was a high stress case for which circuit 4 should have failed. It may suggest that RMS response is not a sufficient metric for fatigue life prediction.

Table 1 Circuit 1 and 4 RMS Fatigue Life

Test	Input RMS (g)	Gage 1 Avg Stress RMS (psi)	Gage 3 Avg Stress RMS (psi)	Circuit 1 Fail Time (min)	Circuit 4 Fail Time (min)
Run01 SN012 DOE01	38.26	837.23	385.05	34.96	34.88
Run02 SN024 DOE09	22.78	778.84	352.80	131.54	131.24
Run03 SN029 DOE03	25.12	1565.92	597.31	21.86	118.65
Run04 SN027 DOE04	43.67	1428.14	656.26	25.19	No Failure
Run05 SN023 DOE14	28.98	945.03	392.74	23.74	17.65
Run06 SN015 DOE02	28.08	834.53	373.62	149.09	148.96
Run07 SN011 DOE07	40.34	1349.84	618.50	13.69	13.72
Run08 SN026 DOE11	40.42	1344.19	605.02	16.90	16.67
Run09 SN030 DOE10	42.35	Gage Failed	377.15	127.37	127.84
Run10 SN017 DOE16	44.27	1250.93	584.05	16.32	36.90
Run11 SN022 DOE15	26.16	1355.01	596.04	22.99	15.99
Run12 SN013 DOE06	42.25	873.58	382.63	50.98	49.33
Run13 SN025 DOE12	30.98	1381.35	654.69	24.31	21.03
Run14 SN018 DOE13	38.93	830.98	397.91	120.55	84.52
Run15 SN016 DOE05	22.6	696.09	327.90	122.98	123.02
Run16 SN020 DOE08	30.88	1261.45	596.76	10.66	9.72
Run17 SN028 DOE07*	25.56	1340.13	672.87	23.97	35.18

The data in Figure 15 are striated. The RMS responses tend to cluster into two populations, one around $\log_{10}(S_{RMS}) = 2.6$ and the other around $\log_{10}(S_{RMS}) = 2.8$ with a large range of cycles to failure for similar response levels. The data points grouped at $\log_{10}(S_{RMS}) = 2.6$ all had low excitation in band C, $110\ Hz < f < 300\ Hz$ (Figure 14). This further suggests that perhaps a richer characterization of the response is needed to model fatigue failure in random vibration.

Table 2 summarizes the moments of the response distributions. Note that the response distributions are not the peak amplitude distributions. The runs that had low excitation in band C are identified with an underline in Table 2. Figure 16 shows an obvious clustering; longer life is associated with larger kurtosis. This suggests that the kurtosis of the response may be a valuable parameter to include in a random vibration fatigue life model.

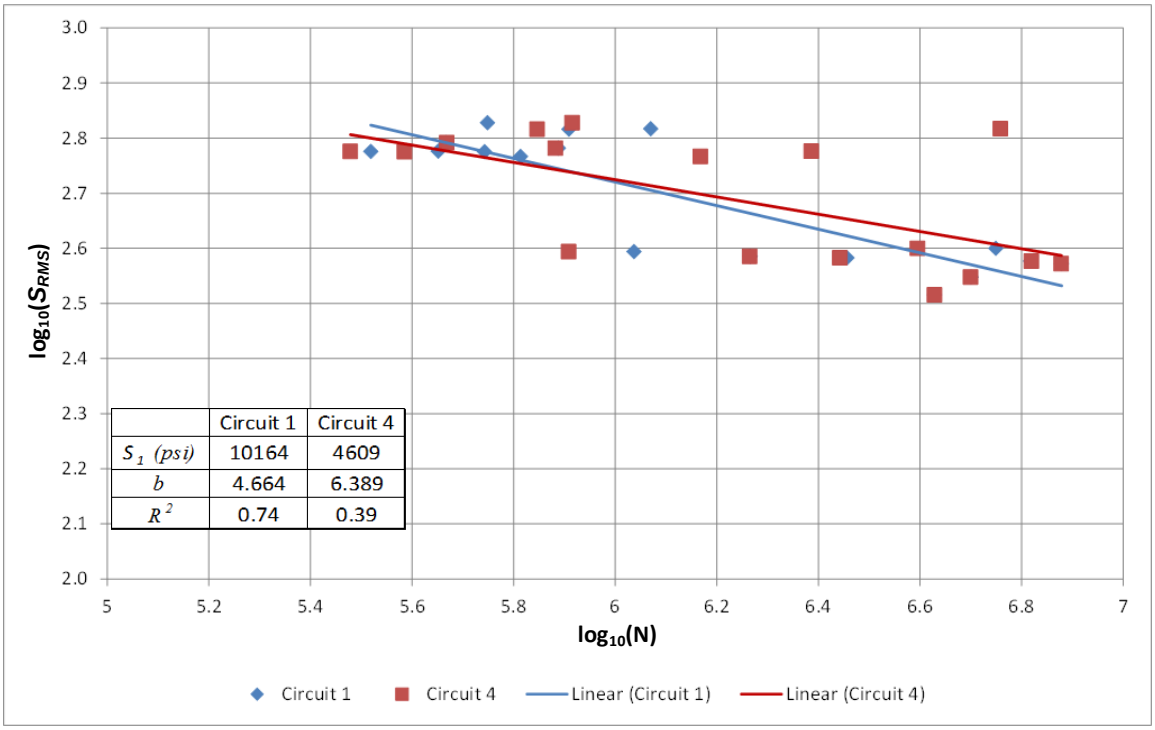

Figure 15 Gage 3 Stress-life Models, Circuit 1 and Circuit 4

Table 2 Gage 3 Average Stress Response Distribution Moments

Test	Input RMS (g)	Gage 3 Avg Stress Mean (psi)	Gage 3 Avg Stress RMS (psi)	Gage 3 Avg Stress Skewness	Gage 3 Avg Stress Kurtosis
Run01 SN012 DOE01	38.26	0.15	385.05	0.12	2.93
Run02 SN024 DOE09	22.78	-3.40	352.80	0.13	2.76
Run03 SN029 DOE03	25.12	-5.54	597.31	0.16	2.47
Run04 SN027 DOE04	43.67	-3.31	656.26	0.15	2.46
Run05 SN023 DOE14	28.98	0.12	392.74	0.17	2.70
Run06 SN015 DOE02	28.08	-5.94	373.62	0.10	2.89
Run07 SN011 DOE07	40.34	-5.65	618.50	0.23	2.62
Run08 SN026 DOE11	40.42	-2.80	605.02	0.16	2.50
Run09 SN030 DOE10	42.35	-2.81	377.15	0.10	2.62
Run10 SN017 DOE16	44.27	0.75	584.05	0.17	2.57
Run11 SN022 DOE15	26.16	-11.28	596.04	0.15	2.57
Run12 SN013 DOE06	42.25	-0.17	382.63	0.13	2.85
Run13 SN025 DOE12	30.98	-5.15	654.69	0.18	2.56
Run14 SN018 DOE13	38.93	-0.31	397.91	0.17	2.77
Run15 SN016 DOE05	22.6	-2.87	327.90	0.12	2.88
Run16 SN020 DOE08	30.88	8.85	596.76	0.19	2.68
Run17 SN028 DOE07*	25.56	-1.11	672.87	0.15	2.49

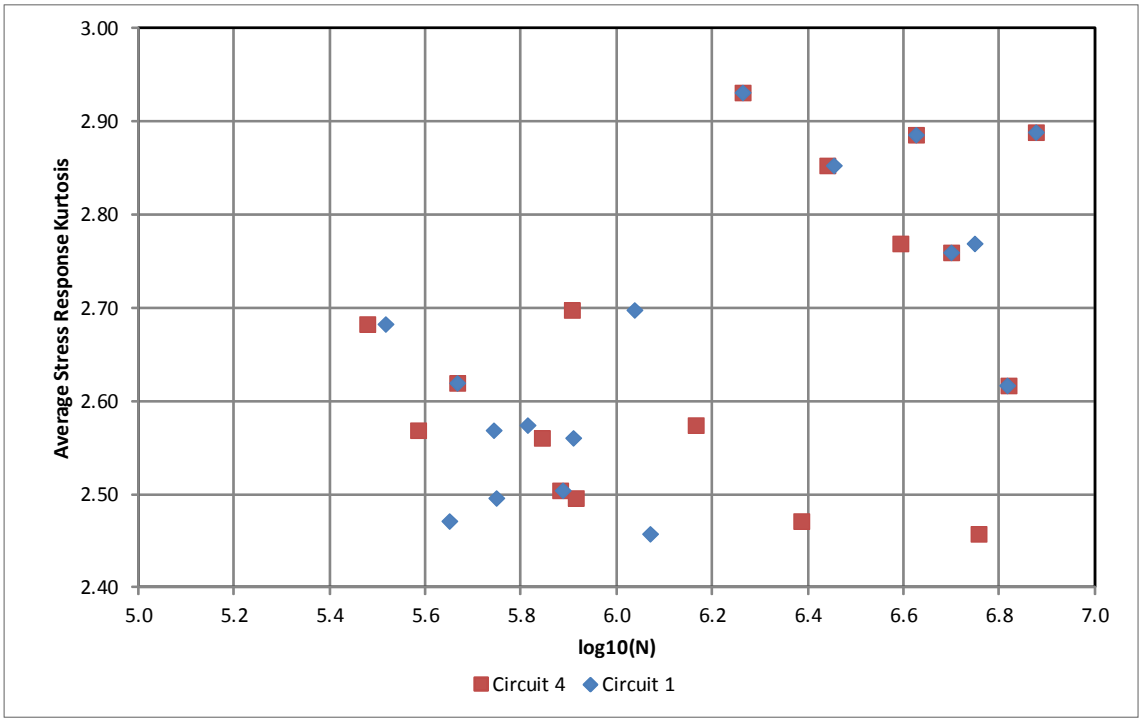

Figure 16 Gage 3 Kurtosis vs. Cycles to Failure

The $\sigma - N_T$ stress life models for circuits 1 and 4 using gage 1 are shown in Figure 17. The stress-life model is consistent with that from gage 1; however, the single cycle flexural strength S_1 is higher, indicative of a higher stress field around gage 1. Since the stress fields are spatially continuous either gage is valid for deriving a stress life model. The differences in the measured stress levels illustrate an important aspect of functional failure fatigue analysis – the measurement location matters.

Figure 18 shows the gage 3 PSD for Run 10, in which the entire bandwidth was excited (i.e. broad band excitation). While the response appears to be dominated by one mode, the distribution of stress amplitudes is nearly Gaussian and the irregularity factor is very small, $\alpha = 0.03$.

Figure 19 shows the stress amplitude distributions from DOE Trial 03 for both rainflow cycles and peak to peak cycles. Run 03 had a high input level in the 110-300 Hz band where the dominant mode resides so it should excite primarily the mode around 200 Hz. The Rice distribution is overlaid on the histograms. While the irregularity factor was the largest for this trial at $\alpha = 0.18$, it is still indicative of a broad band response. The rainflow cycle peak stress amplitude distribution is skewed, whereas the peak-to-peak distribution is nearly symmetric, albeit slightly bi-modal. As discussed in Section IV, this is typical; a rainflow stress distribution generally has a higher percentage of large amplitude cycles than a peak-to-peak distribution. The reason for the bi-modality in the peak-to-peak distribution was not investigated.

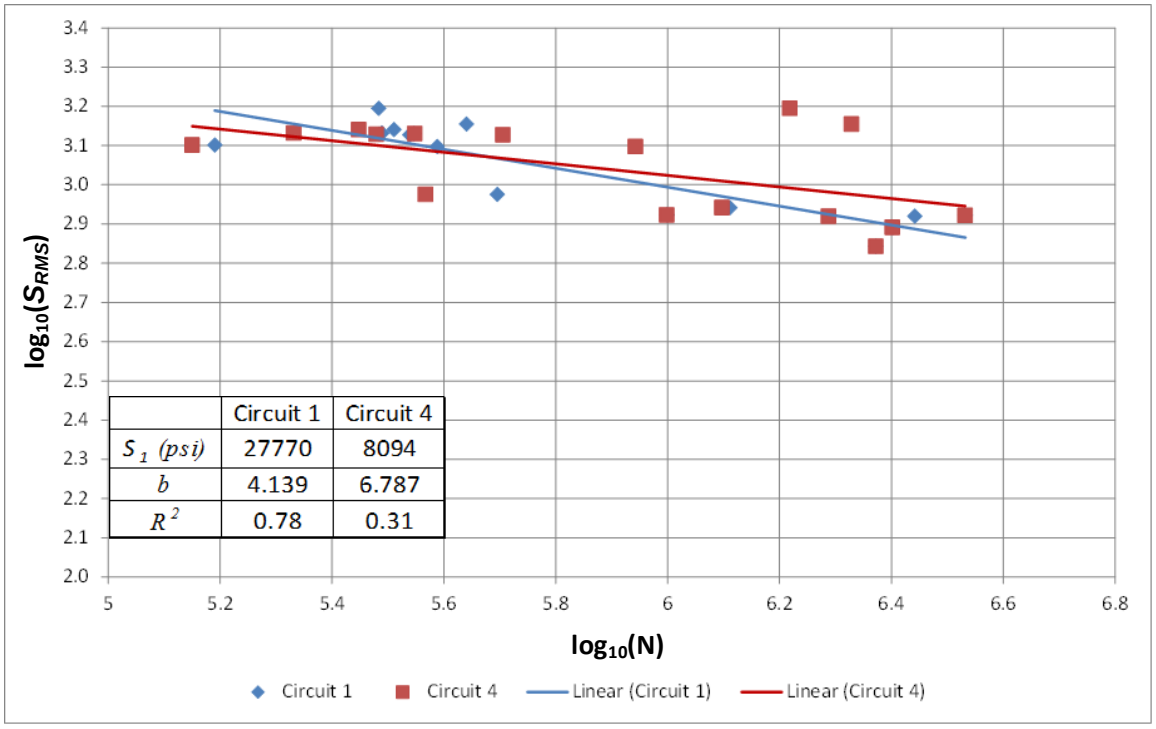

	Circuit 1	Circuit 4
S_1 (psi)	27770	8094
b	4.139	6.787
R^2	0.78	0.31

Figure 17 Gage 1 Stress-life Models, Circuit 1 and Circuit 4

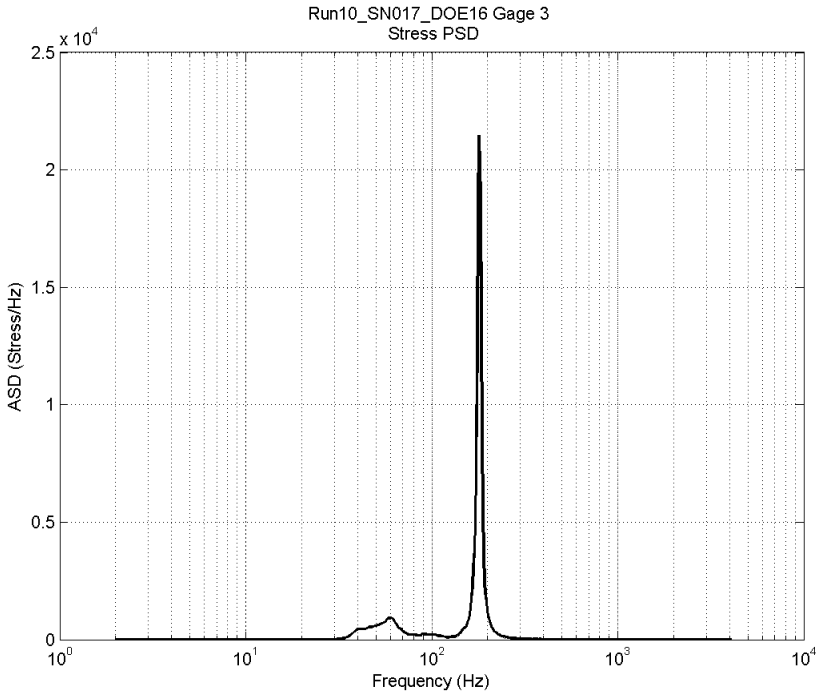

Figure 18 Gage 3 PSD for DOE Trial 16 – Broadband Excitation

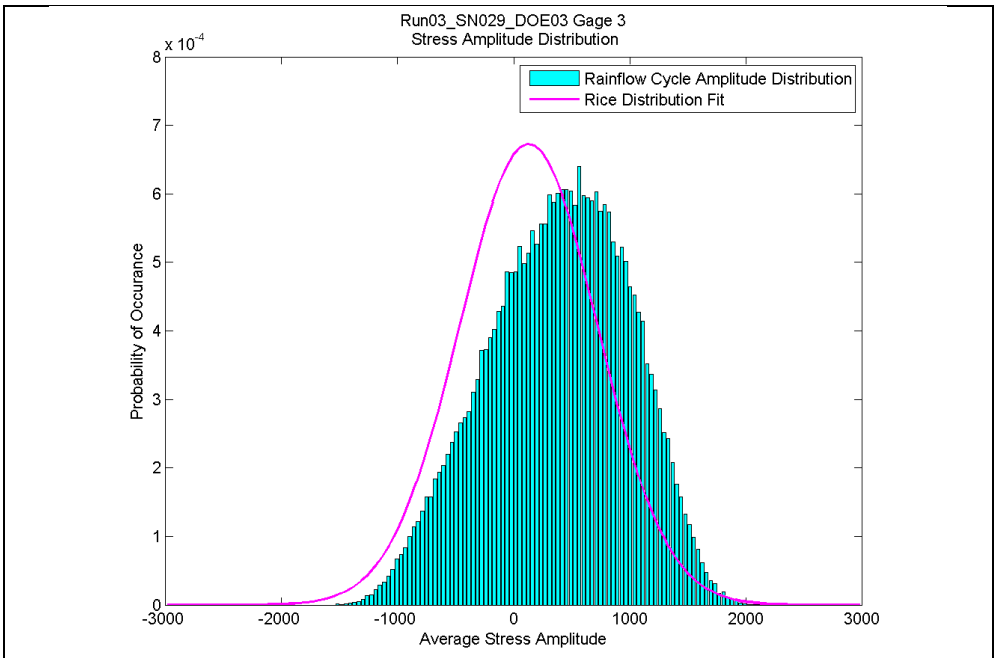

(a) Rainflow Cycle Amplitude Distribution

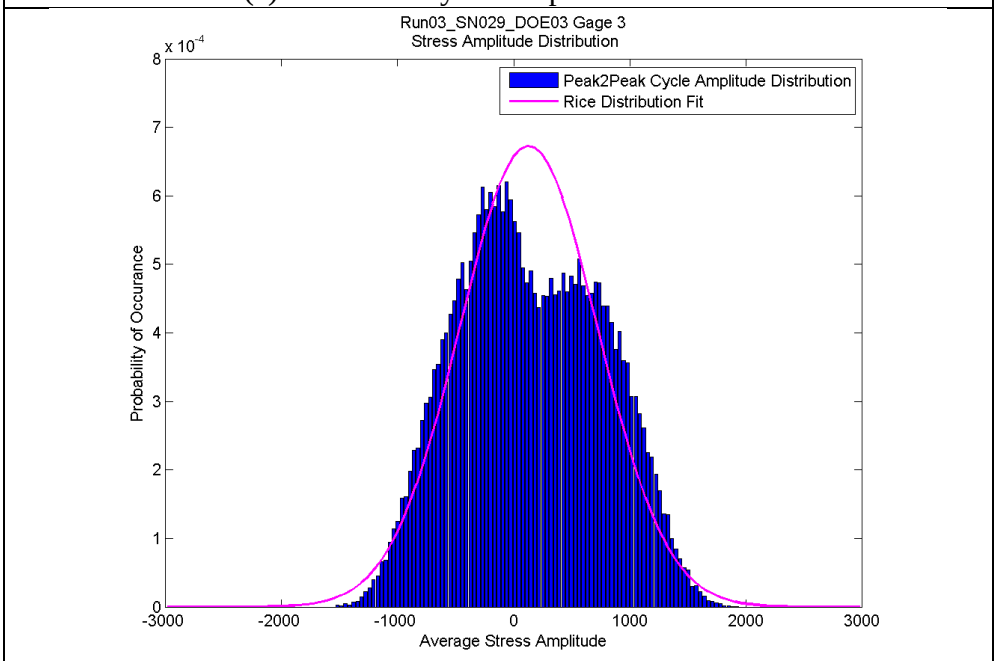

(b) Peak to peak Cycle Amplitude Distribution

Figure 19 Gage 3 Cycle Amplitude Distributions

Figure 20 shows the distributions of cycle means. The measured stresses are about 2% of the flexural strength of FR-4 (70 kpsi) so no correction for mean stress is made. The stress amplitudes can be considered fully reversed stress amplitudes.

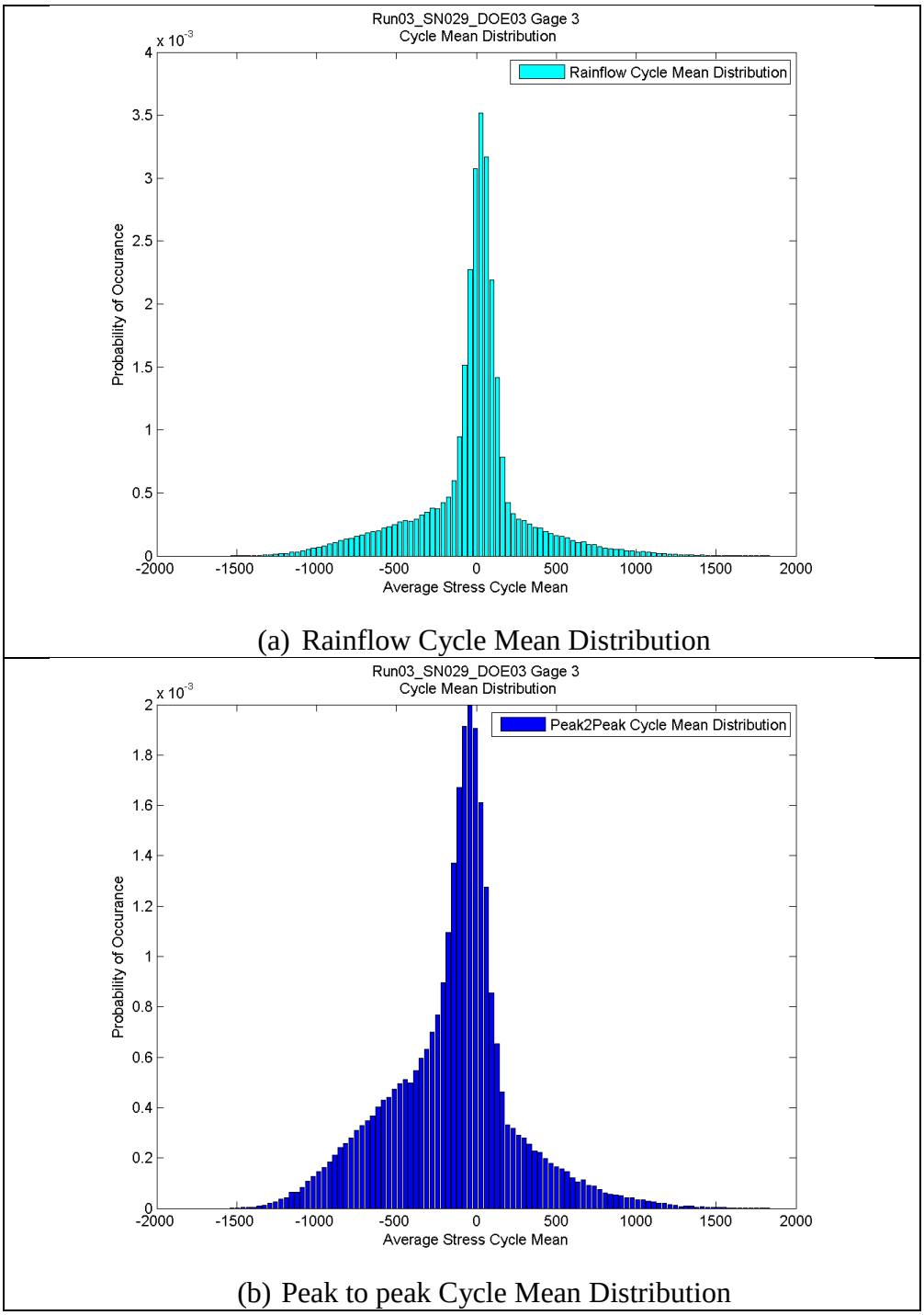

(a) Rainflow Cycle Mean Distribution

(b) Peak to peak Cycle Mean Distribution

Figure 20 Gage 3 Cycle Mean Distributions

A post-test analysis of the circuit 1 failures indicated that they were caused by damage in the FR-4 laminate, not by damage to the electronic components, in this region of the board. Therefore damage accumulated from compression cycles as well as tension cycles. Applying the process outlined previously, Figure 21 shows the derived *S-N* curves based on gage 3, and the model parameters are displayed in Table 3. The figure shows that when creating an *S-N* fatigue life

model from random vibration tests, the narrowband assumption is the least conservative. The *S-N* fatigue life model for the PCB generated with the rainflow cycles was less conservative than the model generated with peak to peak cycles. For a constant number of cycles, the failure stress is higher when estimated with rain-flow cycles. For a constant stress, the estimated number of cycles to failure is larger using a rain-flow definition than the peak-to-peak definition. failure stress is fo for a The Rice distribution model is comparable to the rainflow distribution model. The stress-life model parameters from gage 1 measurements are listed in Table 4.

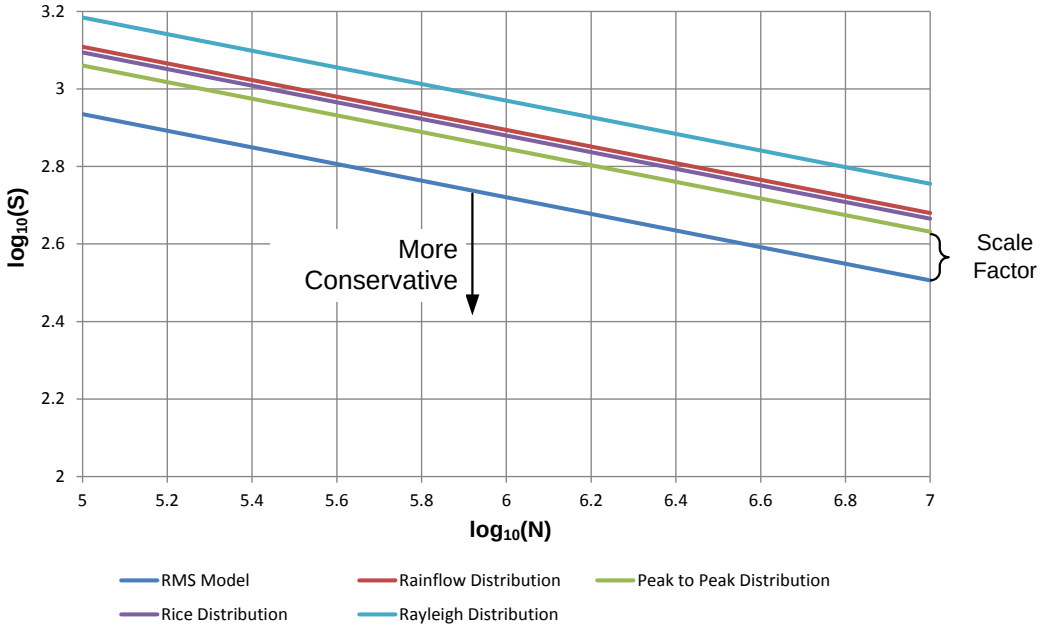

Figure 21 Amplitude Stress-life Model Comparison from Gage 3

Table 3 Circuit 1 Stress-life Model Parameters from Gage 3

	RMS	Rainflow	Peak2Peak	Rice	Rayleigh
S_1 *(psi)*	10164	15166	13570	14666	18047
b	4.664	4.664	4.664	4.664	4.664
λ	1.0	1.48	1.32	1.43	1.76

Table 4 Circuit 1 Stress-life Model Parameters from Gage 1

	RMS	Rainflow	Peak2Peak	Rice	Rayleigh
S_1 *(psi)*	27770	42597	37478	39770	47503
b	4.139	4.139	4.139	4.139	4.139
λ	1.0	1.52	1.34	1.42	1.70

VII. CONCLUSIONS

This paper describes a two-step method to generate power law *S-N* fatigue life models from random vibration data. The first step uses the RMS response to estimate the fatigue life model exponent. The second step estimates the equivalent sinusoidal amplitude that induces the same amount of damage as the random environment and relates it to the RMS response through a scaling factor, which was shown to have an effective range from 1 to 2.5 depending on the stress life model exponent and the distribution of cycle amplitudes.

For a complex structure like the PCB studied in this paper, the failure mode and the location of the "weak link" in the structure should be known. The PCB failure mode was failure in the FR-4, not failure of a surface mounted component. The responses in sixteen excitation cases had broadband characteristics suggesting that a normal distribution of amplitude peaks maybe more often the case than not. Furthermore, the PCB data suggest that additional parameters beyond RMS response, such the kurtosis of the response distribution, should be given consideration when deriving random vibration fatigue-life models.

The narrowband assumption is the least conservative when creating an *S-N* fatigue life model from random vibration tests. The most conservative *S-N* curve is obtained assuming an RMS amplification factor of 1. Using peak-to-peak cycles led to a more conservative *S-N* curve than using rainflow cycles; however the difference was small. The Rice distribution yielded a comparable scaling factor as the rainflow distribution.

When assessing the fatigue failure risk from random vibration with Miner's method and handbook *S-N* curves, the RMS response level must be scaled to obtain an equivalent sinusoidal amplitude. The most conservative approach is to assume a narrowband response which yields the largest scaling factor, but this might be too conservative because the response may be more broadband than narrowband. The Rice distribution is a reasonable approximation if a problem specific distribution is not derived.

REFERENCES

[1] Miner, M.A., "Cumulative Damage in Fatigue," Journal of Applied Physics, 16, A-159, September 1945.

[2] Wirsching, P.H., Paez, T.L., Ortiz, K., *Random Vibrations Theory and Practice*, Dover Publications, 1995, ISBN 0-486-45015-5.

[3] ------, Metallic Materials and Elements for Aerospace Vehicle Structures, MIL-HDBK-5J, January 2003.

[4] Savoie, T. and V. Babuška, "Predicting Fatigue Failure of a Circuit Board in Random Vibration: The Reference Model," 84th Shock & Vibration Symposium, Orlando, FL, November 2013.

[5] Steinberg, D.S., *Vibration Analysis for Electronic Equipment, 2nd Edition*, John Wiley & Sons, 1988, ISBN 0-471-63301-1.

[6] ------, Standard Practices for Cycle Counting in Fatigue Analysis, ASTM Standard E1049-85 (2005).

[7] Downing, S.D. and D.F. Socie, "Simple Rainflow Counting Algorithms," *International Journal of Fatigue*, January 1982, pp. 31-40.

[8] Dowling, N.E., *Mechanical Behavior of Materials: Engineering Methods for Deformation, Fracture, and Fatigue,* Pearson Prentice-Hall, 2007, ISBN 0-13-186312-6.

BIOGRAPHIES

Troy Savoie is a Senior Member of the Technical Staff at Sandia National Laboratories in Albuquerque, NM, in the Program and Test Integration Department where he has worked since 2011. He earned a Ph.D. in Mechanical Engineering in 2010 from the Massachusetts Institute of Technology as a Draper Laboratory Fellow. Dr. Savoie has experience in environmental testing, structural dynamics, risk assessment, statistical design of experiments, optics and signal processing.

Vit Babuska is an Aerospace Engineer and Principal Member of the Technical Staff at Sandia National Laboratories in Albuquerque NM, where he has worked since 2005. He is in the Program and Test Integration Department, which develops test environment specifications for Sandia's systems. He earned his Ph.D. in Aerospace Engineering in 1993 from The University of Texas at Austin. He has worked on various spaceflight programs and spacecraft R&D projects during his career. Two highlights were directing the AFT acoustic test and thermal vacuum tests. Dr. Babuska's experience spans environmental test, structural dynamics, system identification and control of spacecraft systems, and signal processing.